CSIRO PUBLISHING www.publish.csiro.au/journals/eg Copublished paper, please cite all three:
Exploration Geophysics, 2011, **42**, 105–115; *Butsuri-Tansa*, 2011, **64**, 105–115; *Jigu-Mulli-wa-Mulli-Tamsa*, 2011, **14**, 105–115

A poroelastic model for ultrasonic wave attenuation in partially frozen brines

Jun Matsushima[1,4] Takao Nibe[1,2] Makoto Suzuki[1] Yoshibumi Kato[1] Shuichi Rokugawa[3]

[1]Frontier Research Center for Energy and Resources, School of Engineering, The University of Tokyo, 7-3-1 Hongo, Bunkyo-ku, Tokyo 113-8656, Japan.
[2]JGI, Inc., Meikei Building, 1-5-21 Otsuka, Bunkyo-ku, Tokyo 112-0012, Japan.
[3]Department of Technology Management for Innovation, School of Engineering, The University of Tokyo, 7-3-1 Hongo, Bunkyo-ku, Tokyo 113-8656, Japan.
[4]Corresponding author. Email: jun-matsushima@frcer.t.u-tokyo.ac.jp

Abstract. Although there are many possible mechanisms for the intrinsic seismic attenuation in composite materials that include fluids, relative motion between solids and fluids during seismic wave propagation is one of the most important attenuation mechanisms. In our previous study, we conducted ultrasonic wave transmission measurements on an ice-brine coexisting system to examine the influence on ultrasonic waves of the unfrozen brine in the pore microstructure of ice. In order to elucidate the physical mechanism responsible for ultrasonic wave attenuation in the frequency range of 350–600 kHz, measured at different temperatures in partially frozen brines, we employed a poroelastic model based on the Biot theory to describe the propagation of ultrasonic waves through partially frozen brines. By assuming that the solid phase is ice and the liquid phase is the unfrozen brine, fluid properties measured by a pulsed nuclear magnetic resonance technique were used to calculate porosities at different temperatures. The computed intrinsic attenuation at 500 kHz cannot completely predict the measured attenuation results from the experimental study in an ice-brine coexisting system, which suggests that other attenuation mechanisms such as the squirt-flow mechanism and wave scattering effect should be taken into account.

Key words: attenuation mechanism, Biot theory, partially frozen brines, poroelastic, ultrasonic attenuation.

Introduction

Seismic attenuation is a physical parameter representing anelastic behaviour of a rock, controlling both the amplitude decay of seismic waves and the accompanying frequency changes. Although there are many possible mechanisms for the intrinsic seismic attenuation in rocks, including the effects of wetting at grain boundaries (Johnston et al., 1979), viscous shear relaxation (Walsh, 1969), relative motion of the solid frame with respect to fluid inclusions (Biot, 1956), and relative motion at solid boundaries (Walsh, 1966), assessing the most influential mechanism for any given attenuation data is not trivial. Other factors, such as geometrical spreading, wave scattering effects, and source/receiver coupling effects also affect the amplitude and shape of seismic waves. Although seismic attenuation is helpful to estimate physical conditions and rock properties in various fields, the loss mechanisms responsible for seismic attenuation are often unclear and controversial.

Recent advances in seismic methods allow both compressional and shear wave attenuation to be measured. In seismic exploration for methane hydrates (MHs), which are naturally occurring ice-like crystalline solids composed of methane molecules surrounded by water molecules (Sloan, 1990), most previous attempts to detect MH-bearing sediments from seismic data have used seismic velocities (e.g. Wood et al., 1994; Korenaga et al., 1997; Ecker et al., 2000), because MH within the sediment pore space stiffens the sediment and causes an increase in seismic velocity. Intuitively, one would expect the stiffer material to be characterised by higher velocity and lower attenuation. Measurements in many sediments support this intuition (e.g. Klimentos and McCann, 1990). Unexpectedly, significantly large attenuation of seismic waves in MH-bearing sediments has been observed in various geological environments. Guerin and Goldberg (2002) acquired a suite of high-quality downhole logs, and used monopole and dipole waveforms to calculate intrinsic sonic attenuation. In addition, they derived the first empirical relationship between sonic attenuation and MH concentration of sub-permafrost MH-bearing sediments within the Mackenzie Delta, Canada. At the same field, Pratt et al. (2003) used crosshole seismic data with a frequency content of 150–500 Hz to obtain an attenuation tomogram using waveform tomography techniques. The authors also found a strong correlation between attenuation and velocity in the MH-bearing sediments. Matsushima (2005) analyzed attenuation at sonic frequencies of 10–20 kHz for compressional waves and 500–1000 Hz for shear waves, and observed that the presence of MH increases the seismic attenuation of the host sediment. However, Matsushima (2006) used VSP data at the same field to estimate compressional attenuation in MH-bearing sediments at seismic frequencies of 30–110 Hz, and reported that no significant compressional attenuation was observed in MH-bearing sediment. Similarly, Lee (2006) demonstrated, using VSP data, that attenuation of MH-bearing sediment is less than that of water-saturated sediments. These conflicting observations and opposing views of attenuation of MH-bearing sediment are due to various factors. One possible reason is that attenuation in MH-bearing sediments is frequency-dependent. New seismic

© ASEG/SEGJ/KSEG 2011 10.1071/EG10045 0812-3985/11/010105

measurements should be made over a broad frequency range (between seismic and sonic logging frequencies) in various geological environments, to improve our understanding of attenuation of MH-bearing sediment.

However, for a more detailed understanding of the physical mechanism responsible for these attenuation phenomena, laboratory measurements are required. Priest et al. (2006) showed, for the first time, the significant effect of MH on seismic wave attenuation in sand. Priest et al. (2006) also indicated that compressional attenuation is higher than shear attenuation, which differed from field observations (Guerin and Goldberg, 2002; Matsushima, 2005). Further efforts are needed to investigate smaller, pore-scale interactions between grains and infilling material, rather than relying on macroscopic bulk parameters such as velocity or porosity. Prasad and Dvorkin (2004) used partially frozen brine (a mixture of ice and unfrozen brine) to validate attenuation phenomena and to elucidate the physical mechanism responsible for these phenomena in methane hydrate-bearing sediments. Spetzler and Anderson (1968) used the same simple two-phase system (ice and unfrozen brine) to study the effects of temperature and partial melting in the upper mantle low-velocity zone. To study the attenuation characteristics due to partial melting at the grain boundaries of mantle rocks, Gao et al. (1993) measured the attenuation of aluminium samples and its changes after the invasion of a small quantity of gallium, which has a eutectic temperature of 27°C. The advantage of employing a simple two-phase system is that by varying the temperature the amount of the liquid phase can be controlled.

In a previous paper, Matsushima et al. (2008) used partially frozen brine as a solid-liquid coexistence system to investigate attenuation of ultrasonic waves. Ultrasonic wave transmission measurements on this ice-brine coexisting system were conducted to examine the influence of unfrozen brine in the pore microstructure of ice on ultrasonic waves. They observed variations in the transmitted waves in the frequency range of 150–1000 kHz as the temperature of the system was changed from 20°C to −15°C, varying the material properties from liquid a solid-liquid mixture. They quantitatively estimated the attenuation in a frequency range of 350–600 kHz by considering different distances between the source and receiver transducers. Additionally, they estimated the total amount of unfrozen brine at each temperature by a pulsed nuclear magnetic resonance (NMR) technique and related it to the measured attenuation results. Their waveform analyses indicated that ultrasonic attenuation in an ice-brine coexisting system reaches its peak at a temperature of −3°C, where the ratio of the liquid phase to the total volume is maximised at ~85%. Although their observations did not indicate a plausible mechanism for attenuation in an ice-brine coexisting system, their observations demonstrate that fluid in a permeable system plays an important role in attenuating elastic waves.

Theoretical models will be helpful to elucidate the physical mechanism responsible for ultrasonic wave attenuation in partially frozen brines. Carcione et al. (2007) modified Biot's poroelastic model (Biot, 1956) to describe the propagation of ultrasonic waves through partially frozen orange juice. They predicted the degree of freezing of orange juice using the wave velocity and attenuation factor. Their theoretical results were compared with the experimental results obtained by Lee et al. (2004). Additionally, Carcione and Seriani (2001) proposed a numerical algorithm to simulate wave propagation in frozen porous media where the pore space is filled with ice and water. Their model is based on a Biot-type theory and predicts compressional and shear wave attenuations. Furthermore, Carcione et al. (2003) extended this algorithm to simulate wave propagation in a frozen porous medium with fractal variations of freezing conditions. Leclaire et al. (1994) expanded Biot's model to analyse wave propagation in frozen porous media such as frozen soil and permafrost. In their model, ice particles and liquid water coexist, and elastic waves propagate through a three-phase mixture of a solid grain matrix, liquid water, and a solid ice matrix. A Biot-type theory and its expansion may be helpful to theoretically explain the attenuation phenomenon in partially frozen brines. In the present paper, we applied a similar theoretical approach by using the same poroelastic model as Carcione et al. (2007) to describe the propagation of ultrasonic waves through partially frozen brines.

Poroelastic model for partially frozen brine

Generation of partially frozen brine

During the growth of ice from brine, salt cannot be incorporated into the ice crystals. As the ice freezes, the salt is rejected and concentrates in the brine; thus, as the salinity increases in the brine-filled pores, the freezing point of the remaining fluid is successively lowered. Some of this brine drains out through the channels as the ice grows, but much of the brine remains trapped between the ice crystals. In this system, the amount of unfrozen brine depends on the temperature and NaCl concentration. Hence, the amount of unfrozen brine can be controlled by varying the temperature. However, we do not measure the salinity of unfrozen brines at each temperature because the spatial variation of the salinity is considered to be large. Matsushima et al. (2008) measured the amount of unfrozen water using an NMR technique, which provided valuable information about the distribution of ice and unfrozen brine in an ice-water coexisting system. Furthermore, they categorised the unfrozen brine into two components: low-mobility brine and high-mobility brine. In the case of low-mobility brine, unfrozen brine is trapped in smaller pore spaces than in the case of high-mobility brine. In such small pore spaces, the collision of water molecules with the walls of the enclosing pore reduces the effective Brownian motion (Callaghan et al., 1999). The NMR measurements by Matsushima et al. (2008) demonstrated that the total amount of unfrozen brine increases with increasing temperature from −15°C to −3°C, which is interpreted as increase in pore size. Additionally, they demonstrated that the ratio of low-mobility to high-mobility brines increases as the temperature decreases, which can be interpreted as reduction in the pore connectivity.

Percolation theory and elastic modulus

Assuming that the solid phase is ice and the liquid phase is the unfrozen brine, we use the same poroelastic model (modified Biot model) as Carcione et al. (2007) to describe the propagation of ultrasonic waves through partially frozen brines. Figure 1 shows a schematic diagram of poroelastic modelling based on Carcione et al. (2007). First, the shear and bulk moduli of the matrix formed by the ice phase were derived by percolation theory, which can be used to describe the transition of a system or a material between continuous and discontinuous states (Leclaire et al., 1994). De Gennes (1976) derived the scaling law by assuming that the behaviour of elasticity is analogous to that of electrical conductivity in a random register network. During this process, which is called transition of percolation, connections appear or disappear between elements of the system or material. In the case of elasticity, momentum is transported. The behaviour of the system can be described by the exponent τ where $\kappa \propto (p-p_c)^{\tau}$ is the elastic modulus, p represents the occupied bonds or sites, and p_c is the percolation threshold value of p (Deptuck et al., 1985). Leclaire et al. (1994) derived the following relation for three

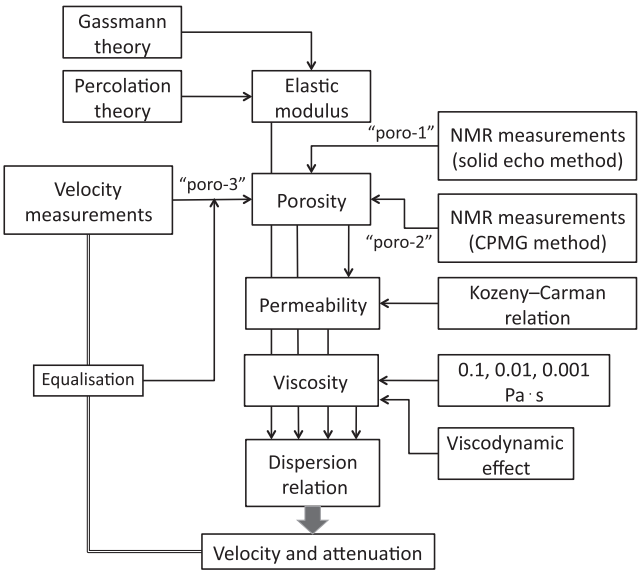

Fig. 1. Schematic diagram of the poroelastic modelling process, based on Carcione et al. (2007).

phases composed of sediments grains, pore fluid, and ice, based on percolation theory:

$$G_m = G_{\max}\left(\frac{\phi_{\text{ice}}}{\phi}\right)^{3.8}, \tag{1}$$

$$K_m = K_{\max}\left(\frac{\phi_{\text{ice}}}{\phi}\right)^{3.8}, \tag{2}$$

where G_m and K_m are the shear and bulk moduli of the ice matrix, respectively. ϕ is the formation porosity, ϕ_{ice} is the volumetric fraction of ice, $G_{\max}$ and $K_{\max}$ are the maximum shear and bulk moduli of ice matrix for $\phi_{\text{ice}} = \phi$, respectively. Carcione et al. (2007) modified equations 1 and 2 for a two-phase system composed of unfrozen liquid and ice as:

$$G_m = G_{\text{ice}}(1-\phi_w)^{3.8}, \tag{3}$$

$$K_m = K_{\text{ice}}(1-\phi_w)^{3.8}, \tag{4}$$

where G_{ice} and K_{ice} are the shear and bulk moduli of ice, respectively, and ϕ_w is the proportion of unfrozen water. The density of the frozen porous medium is:

$$\rho = (1-\phi_w)\rho_{\text{ice}} + \phi_w\rho_w, \tag{5}$$

where ρ_{ice} and ρ_w are the ice and water densities, respectively. The following mathematical development is based on Carcione et al. (2007).

Dispersion relation

The complex velocity of P-waves (v_c^p) can be obtained from the following fourth-order equation, which is derived from the dispersion relations (e.g. Stoll, 1977):

$$a v_c^{p4} + b v_c^{p2} + c = 0. \tag{6}$$

The coefficients in equation 6 are given by:

$$a = -\left(\rho_w^2 + \frac{i}{\omega}Y(\omega)\rho\right) \tag{7}$$

$$b = \frac{i}{\omega}Y(\omega)E_G + \frac{K_{\text{ice}}(2\alpha\rho_w - \rho)}{1-\phi_w - K_m/K_{\text{ice}} + \phi_w K_{\text{ice}}/K_w}, \tag{8}$$

$$c = \frac{E_m K_{\text{ice}}}{1-\phi_w - K_m/K_{\text{ice}} + \phi_w K_{\text{ice}}/K_w}, \tag{9}$$

where E_m, E_G, α are the P-wave modulus of the ice frame, the Gassmann P-wave modulus, and the Biot effective stress coefficient, respectively. These can be calculated from:

$$E_m = K_m + \frac{4}{3}G_m, \tag{10}$$

$$E_G = K_G + \frac{4}{3}G_m, \tag{11}$$

$$\alpha = 1 - \frac{K_m}{K_{\text{ice}}}, \tag{12}$$

where K_G is Gassman's low-frequency bulk modulus of the partially frozen medium, defined by the low-frequency Gassmann theory (Gassmann, 1951). $Y(\omega)$ in equations 7 and 8 is the viscodynamic term described by the following section.

Viscodynamic effect

The viscodynamic term expressed by the following equation 13 is important at high frequencies, because while the frame and pore fluid move in phase and coupling between solid and fluid components is at maximum at low frequencies, relative motion between pore fluid and frame are significant at high frequencies. The assumption of an ideal Poiseuille flow (laminar flow) is valid for lower frequencies, that is, the fluid motion is dominated by viscous effects, but at high frequencies fluid motion is dominated by inertial effects, which result in lower viscosity. The viscodynamic term can take these effects into account:

$$Y(\omega) = i\omega\left(\frac{\rho_w\tau}{\varphi_w}\right) + \frac{\eta F(\omega)}{\kappa}, \tag{13}$$

where η is the water viscosity and κ is the permeability derived from the Kozeny–Carman relation (Kozeny, 1927; Carman, 1937) expressed as:

$$\kappa = \frac{2\kappa_0\phi_w^3}{(1-\phi_w)^2}, \tag{14}$$

where κ_0 is a reference value at 50% water proportion. In this work we have used 2.5 Darcy, which is a value commonly used for materials with relatively high porosity (Carcione et al., 2007).

τ in Eqn (13) is the tortuosity of the pore space, which is given by:

$$\tau = 1 + \beta\left(\frac{1}{\phi_w} - 1\right). \tag{15}$$

Although tortuosity is defined as the square of the ratio of total flow-path length to length of the sample, an approximate relation shown by equation 15 between the porosity and the tortuosity has been proposed (e.g. Berryman, 1980). The value of β must be calculated from a microscopic model of the frame moving in the fluid. Although we should carefully determine the value for the case of our ice-brine coexisting system, here we have used the same value $\beta = 0.02$ as Carcione et al. (2007) used.

$F(\omega)$ in equation 13 is the viscosity correction term expressed by the following equation:

$$F(\omega) = \sqrt{1 - \frac{4i\tau^2\kappa}{x\Lambda^2\phi_w}},$$

$$x = \frac{\eta\phi_w}{\omega\kappa\rho_w}, \tag{16}$$

$$\Lambda = \sqrt{\frac{\xi\tau\kappa}{\phi_w}}.$$

where Λ is a geometrical parameter defined by Johnson et al. (1987), with $2/\Lambda$ being essentially the surface-to-pore-volume

ratio of the pore-solid interface. The parameter ξ describes the shape of pore network, with $\xi = 8$ for the case with a set of non-intersecting canted tubes (Carcione et al., 2007).

Solution of equation

Finally, as the solution of the quadric equation 6, we obtained two complex roots, v_c^{p+}, v_c^{p-}, which correspond to Biot's fast and slow P-waves, respectively. The phase velocities are given by the following equation:

$$v_{p\pm} = \frac{1}{\mathrm{Re}\left(\frac{1}{v_c^{p\pm}}\right)}. \tag{17}$$

Quality factors are expressed as:

$$Q_{p\pm} = \frac{\pi f}{\alpha_{p\pm} v_{p\pm}}, \tag{18}$$

where $\alpha_{p\pm}$ are the attenuation factors given by the following equation:

$$\alpha_{p\pm} = -2\pi f \ \mathrm{Im}\left(\frac{1}{v_c^{p\pm}}\right). \tag{19}$$

Table 1 lists the physical properties used in the present study. The elastic moduli of pure ice and water are taken from Carcione et al. (2007). The viscosity of brine is a function of salinity and temperature; that is, the viscosity of brine increases with increasing salinity and with decreasing temperature. The viscosity of water at 20°C is ~0.001 Pa.s. Carcione et al. (2007) used a high and constant viscosity value (0.1 Pa.s) because they assumed that the presence of sugars in the liquid and the low temperature would raise viscosity. However, they described the requirement for a better description of the effect of temperature on viscosity, because decreasing temperatures lead to increasing viscosity due to increasing sugar concentrations in the unfrozen juice solution. Here we have used three different values of viscosity: 0.001, 0.01, and 0.1 Pa.s.

Results

Determination of porosity

Figure 2 shows the results of experiments to determine the porosity of partially frozen brine as a function of temperature. Three different values for porosity have been measured at each temperature. Matsushima et al. (2008) estimated the total amount of unfrozen brine at each temperature using a pulsed NMR technique. The NMR experiment consists of measuring the rate at which each proton relaxes to an initial equilibrium position after the magnetisation is temporarily oriented to another unstable direction by a radio-frequency pulse. NMR focuses on protons in the fluid phase. Thus, the measured relaxation rate is related to the movable water in the water-filled pore space. Matsushima et al. (2008) applied two types of pulsed NMR methods. The first is the solid echo method, which was used to estimate the total amount of unfrozen brine. In this case, the porosity is calculated as the ratio of the unfrozen brine to the total volume in an ice-brine coexisting system. These values are denoted by the solid triangles in Figure 2. We hereafter call this case 'poro-1'. The second NMR method is the Carr-Purcell Meiboom-Gill (CPMG) method (Carr and Purcell, 1954; Meiboom and Gill, 1958), which is used to categorise the unfrozen brine into two components: low-mobility brine and high-mobility brine. Low-mobility brine is unfrozen brine that is trapped in smaller pore spaces than high-mobility brine. In this case, the porosity is calculated as the ratio of the unfrozen brine with a high mobility to the total volume in an ice-brine coexisting system (denoted by the solid squares in Figure 2). We hereafter call this case 'poro-2'. The porosity curve denoted by solid circles in Figure 2 is derived from observed velocities in the experiments by Matsushima et al. (2008), which are described in detail later. We hereafter call this case 'poro-3'.

Table 1. Material properties used in numerical simulations and the poroelastic model.

Physical parameters	Given value
Ice bulk modulus	8.5 GPa
Ice shear modulus	3.7 GPa
Ice density	920 kg/m^3
Water bulk modulus	2.25 GPa
Water density	1020 kg/m^3
Viscosity of brine	0.001, 0.01, 0.1 Pa.s
β	0.02
Reference permeability	2.5 Darcy

Calculation of velocity

Figure 3*a* and *b* compare the experimental P-wave velocities in the frequency range of 350–600 kHz to the calculated results at 500 kHz, for two different porosity values and three different viscosity values (0.001, 0.01, and 0.1 Pa.s) at temperatures between −15°C and −3°C. Although both the calculated and measured velocities increase with decreasing temperature, the rate of the increase for the measured velocities is lower than that of calculated velocities. We can also see that the difference between calculated and measured velocities in the case of poro-1 (Figure 3*a*) is larger than that of poro-2 (Figure 3*b*). The calculated velocities shown in Figure 3*b* are almost similar to measured velocities below −12°C while there are significant differences between them

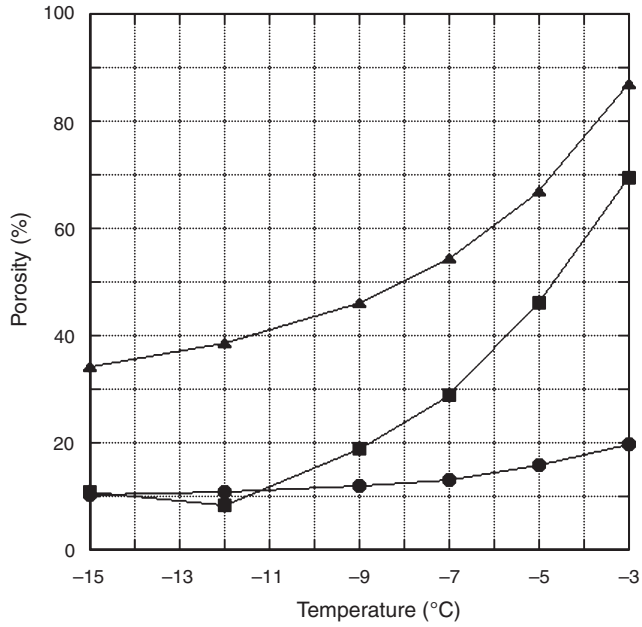

Fig. 2. Solid triangles ('poro-1' case): porosity of partially frozen brines at each temperature, calculated as the ratio of the frozen brine to the total volume in an ice-brine coexisting system using NMR measurements (the solid echo method); solid squares ('poro-2' case): porosity of ice at each temperature calculated as the ratio of the liquid phase with high mobility to the total volume in an ice-brine coexisting system using NMR measurements (Carr-Purcell Meiboom-Gill method); solid circles ('poro-3' case): porosity derived from observed velocities (Matsushima et al. 2008).

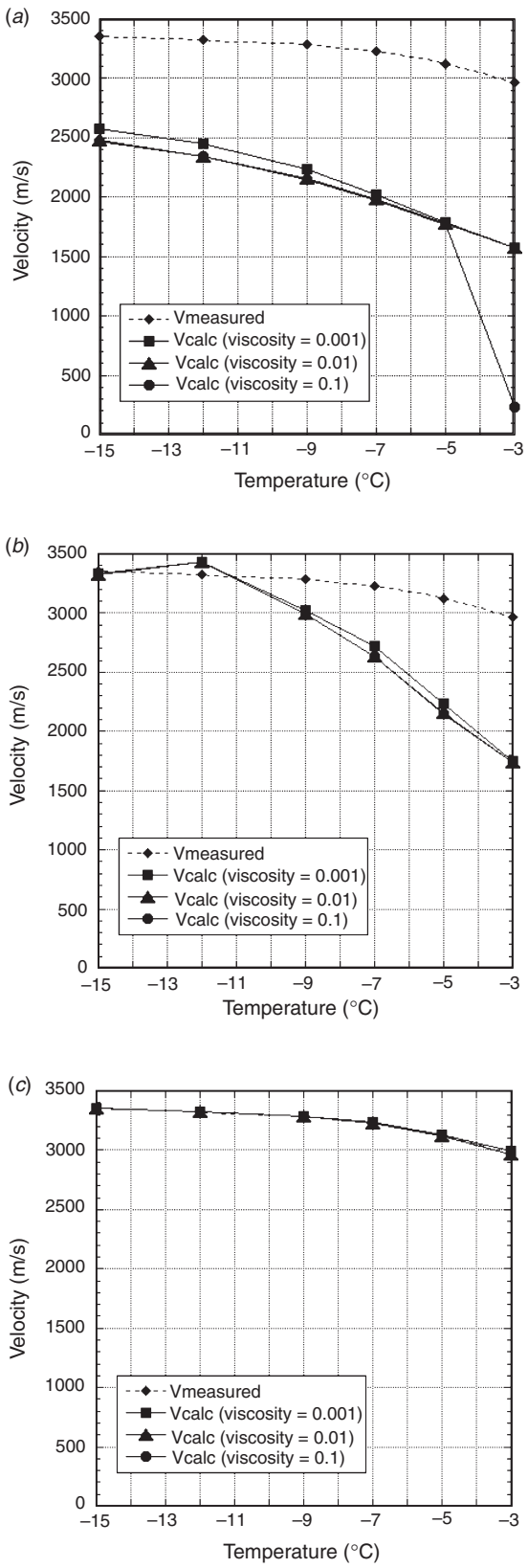

Fig. 3. Comparison between the calculated (dotted lines) and experimentally measured P-wave velocities (solid lines) versus temperature from −15°C to −3°C. Calculated P-wave velocities are obtained by a poroelastic model at 500 kHz, while the measured velocities obtained by Matsushima et al. (2008) are determined by selecting the arrival time from the observed waveforms and dividing this time by the source/receiver distance. Solid squares: viscosity = 0.001 Pa.s; solid triangles: viscosity = 0.01 Pa.s; solid circles: viscosity = 0.1 Pa.s. Panel a: 'poro-1' case; panel b: 'poro-2' case; panel c: 'poro-3' case.

even below −12°C in Figure 3*a*. In Figure 3*c* we determined porosities at each temperature to fit the calculated to measured velocities. The porosity curve denoted by solid circles in Figure 2 (the poro-3 case) is the result of this adjustment procedure. We can see that the porosities determined by NMR are larger than those determined by velocities.

There may be some reasons for the discrepancies between these observations. One possible reason is that size of samples used for ultrasonic measurements was different from that used for NMR measurements. Because of limited space of the NMR measurement room, we were not able to use the same plastic container (80 × 130 × 150 mm) used in laboratory waveform measurements. According to visual and tactile observations, the ice-brine coexisting system comprises a group of thin ice plates. Such a system develops well in the plastic container used in ultrasonic measurements, even at a temperature of −3°C. Although we chose the same time schedule for cooling in both cases, the ice-brine systems generated in different size containers are expected to differ from each other. Each ice-brine coexisting system exhibits a spatial variation in stiffness, in that the upper part is harder than that of the lower part because ice forms from the upper part to the lower part. These variations in the stiffness of the ice-brine coexisting system might refract seismic energy through the harder parts, resulting in higher observed velocities.

Another possible reason is the accuracy of categorising the partially frozen brines into liquids and solids, or into low and high mobility. This operation may cause the overestimation of the amount of liquid phase. In the NMR analysis, we roughly categorised the fluid into two components (i.e. the biexponential case). Further careful categorisation using a multi-exponential expression representing a distribution of T_2 (transverse relaxation times) is needed to characterise the sample fluid distribution. Furthermore, we can see that three porosity curves did not produce significant differences of velocity values except for the case of poro-1 (Figure 3*a*) with viscosity = 0.1, where the physical process is diffusive rather than elastic because of extremely high porosity (more than 85%) and high viscosity.

Calculation of attenuation

Figure 4 compares the experimental P-wave attenuation measurements in the frequency range of 350–600 kHz to the calculated results at 500 kHz for three different porosity curves and three different viscosity values, at temperatures between −15°C and −3°C. The attenuation curve for the measured data is derived by averaging the measurements with different waveforms and source/receiver configurations. Because attenuation estimates depend on window length, Matsushima et al. (2008) used two types of direct-arrival extraction (two cycles, three cycles), with different source/receiver distance pairs, for attenuation analysis. The measured attenuation results shown by the dotted lines in Figure 4 are the average for the extracted first arrival waveforms for both two cycles and three cycles, with error bars which are the standard deviation for the six different source/receiver distance pairs (2–4 cm, 2–5 cm, 2–6 cm, 3–5 cm, 3–6 cm, and 4–6 cm). In Figure 4, the measured attenuation results (dotted line) reach their peak at a temperature of −3°C and gradually decrease with decreasing temperature. At a temperature of −3°C, the ratio of the liquid phase to the total volume is maximum, as shown in Figure 2. However, the calculated attenuation results (solid line) reach their peak at different temperatures. This can be explained by the viscodynamic effect, which depends on frequency. The distinction between high and low frequencies

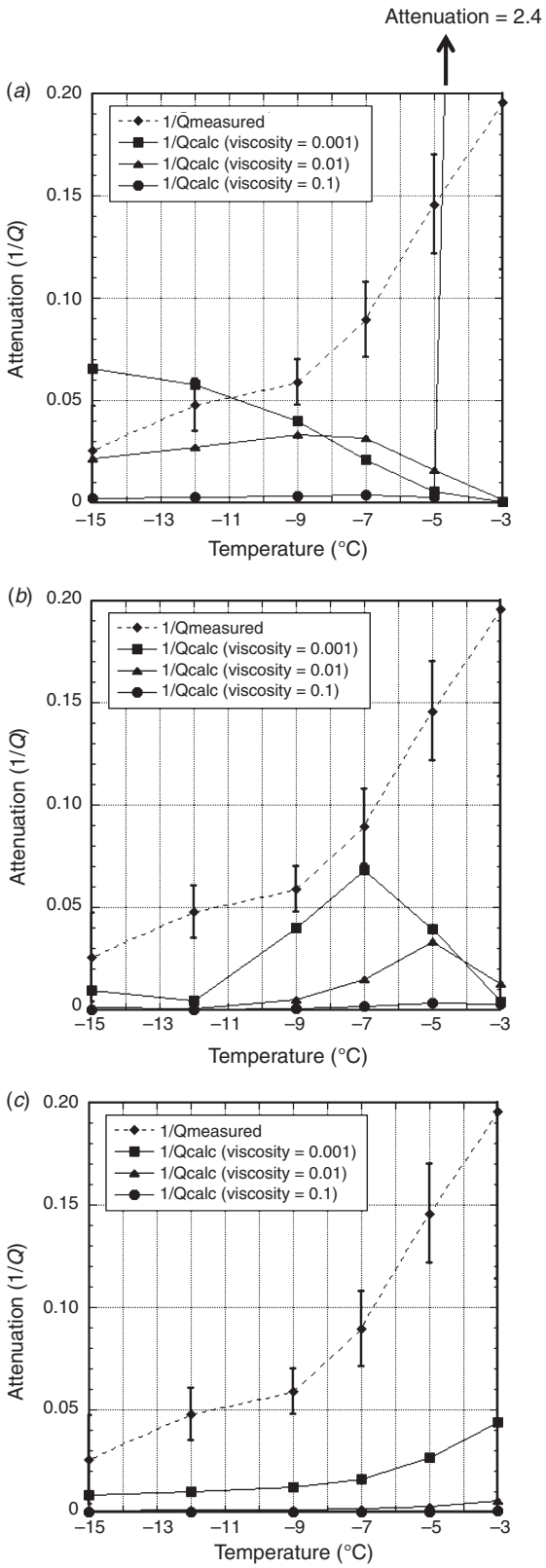

Fig. 4. Comparison between the calculated (dotted lines) and experimentally measured P-wave attenuation ($1/Q$) (solid lines) versus temperature from −15°C to −3°C. Calculated P-wave attenuation is at 500 kHz, while the experimentally observed attenuation is from Matsushima et al. (2008), in a frequency range of 350–600 kHz with different windows (two cycles and three cycles) of direct arrivals. Error bars of the experimentally observed attenuation are the standard deviations of different source/receiver distance pairs. Solid squares: viscosity = 0.001 Pa.s; solid triangles: viscosity = 0.01 Pa.s; solid circles: viscosity = 0.1 Pa.s. Panel a: 'poro-1' case; panel b: 'poro-2' case; panel c: 'poro-3' case.

is whether the viscous skin depth defined as $(2\eta/\rho_w\omega)^{1/2}$ is small or large compared to the sizes of the pores (Johnson et al., 1987). When the rock frame is accelerated by an acoustic wave, shear stresses are generated within the pore fluid. These stresses decay exponentially away from the pore wall with a viscous skin depth that decreases with increasing frequency. At low frequencies the skin depth is much larger than the pore diameter, shear stresses are small, and viscous energy dissipation is minimal. At high frequencies the skin depth is very small, creating large shear stresses in a very small volume near the pore wall. Again, energy dissipation is small. However, at intermediate frequencies where the viscous skin depth is comparable to the pore size, moderate shear stresses exist throughout the pore volume and maximum energy dissipation occurs (Winkler and Nur, 1982).

We can see that the calculated attenuations for all viscosity cases are smaller than the actual measurements in the laboratory. This may indicate that the poroelastic model used in the present study cannot completely represent the attenuation of ultrasonic waves in real samples. As described in the previous section, each ice-brine coexisting system exhibits spatial variation in stiffness. The gradual variations in stiffness in the ice-brine coexisting system may refract seismic energy to harder parts, resulting in a decrease in observed attenuation. Thus, in the case of attenuation, the different size of samples between ultrasonic measurements and NMR measurements may not be a possible reason for discrepancy between calculated and observed results. However, we should also note the uncertainty in NMR measurements described in the previous section. Furthermore, we can see the anomalous attenuation value (2.4) for the poro-1 case with viscosity = 0.1 (Figure 4*a*). As described above, the physical process is diffusive rather than elastic because of extremely high porosity (more than 85%) and high viscosity.

Uncertainty of experimental data

As described above, the dotted lines with error bars in Figure 4 show the variation in attenuation results with different window size and different source/receiver distance pairs. The effect of windowing degrades the attenuation estimates, and the estimates are dependent on window length (Sams and Goldberg, 1990). The estimated spectrum can be significantly biased by spectral leakage. Here we estimate the uncertainty of observed data in laboratory experiments. Matsushima et al. (2008) verified the performance of the transducers at low temperatures to find that the coefficient of variation (CV) of reproducibility of velocities, average frequencies, and peak-to-peak amplitudes is very small, that is, the CV of each parameters is 0.36, 0.30, and 1.94%, respectively. Furthermore, Suzuki et al. (2010) verified the performance of a piezoelectric transducer under confined pressure during the generation of ice crystals to observe that the variation of velocities, average frequencies, and peak-to-peak amplitudes is at most 0.4, 1.6, 200.0%, respectively. Although the variation of peak-to-peak amplitudes is very large, this does not significantly disturb attenuation results because the attenuation analysis method adopted here depends on the ratio of amplitudes. Suzuki et al. (2010) also examined the period of freezing time required until stable waveforms are obtained at each temperature, and concluded that the freezing time at each temperature adopted in Matsushima et al. (2008) is appropriate for obtaining reliable waveform data.

In terms of repeatability of waveform data, the reproducibility of the ice-brine system is the most essential factor because the ice-brine coexisting systems are expected to be generated differently at different times. Figure 5*a–d* show the repeatability of twice-recorded waveform data at 0°C, −5°C, −9°C, and −15°C, while

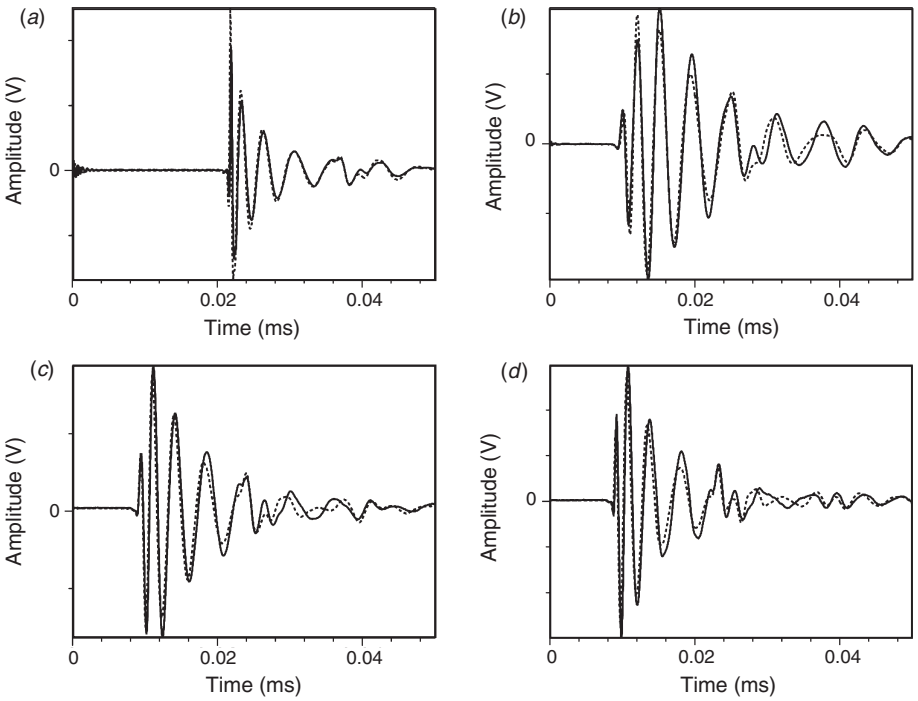

Fig. 5. Repeatability of twice-recorded waveform data at (*a*) 0°C, (*b*) −5°C, (*c*) −9°C, and (*d*) −15°C.

Figure 6*a–d* show the Fourier amplitude spectra for the waveforms shown in Figure 5*a–d*, respectively. In Figures 5 and 6, solid and dotted lines indicates the first and second measurements, respectively. We can see that several cycles from the onset of the direct arrival of waveforms are repeatable while there are small but significant differences in the wave trains following the direct waves after generation of the ice-brine coexisting system (i.e. at temperatures below −5°C). We interpret these small differences to be due to scattering effects caused by local heterogeneities in the ice-brine coexisting system. Anyhow, according to our careful investigation with multiple data measurements, we believe that the waveforms measured for attenuation estimation are repeatable.

Discussion

Many existing rock-physics models for attenuation are based on the Biot model (Biot, 1956) and its extension, because the physical interactions between grains and pore fluids are considered to greatly contribute to seismic attenuation in rocks (e.g. Leclaire et al., 1994). Biot (1956) has established a semi-phenomenological theory for the propagation of elastic waves in

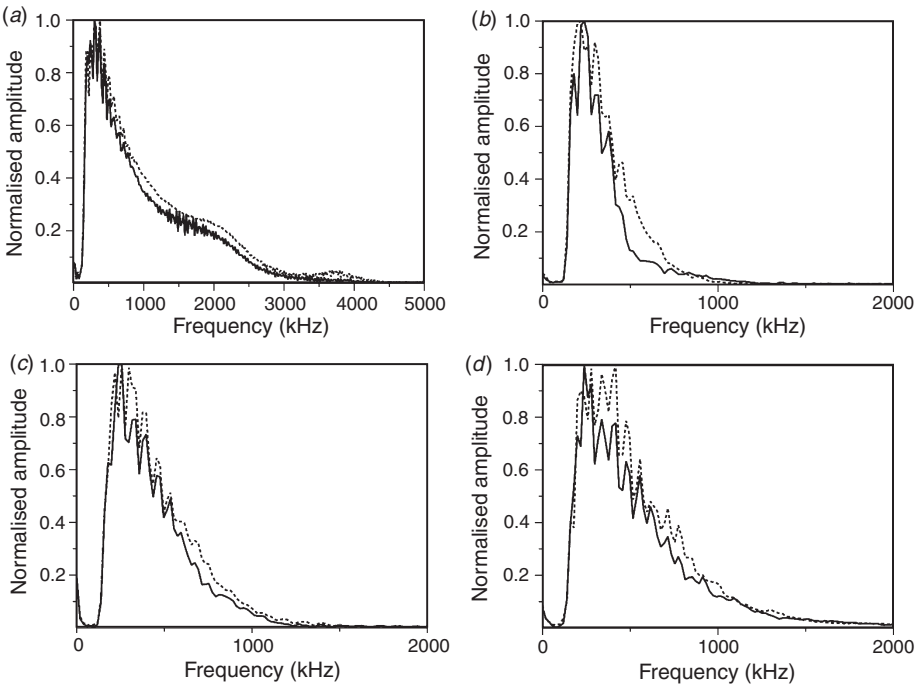

Fig. 6. Normalised Fourier amplitude spectra for the waveforms shown in Figure 5. The amplitude scale is normalised by maximum value.

fluid-saturated porous media. The Biot model has been confirmed theoretically (e.g. Burridge and Keller, 1981) and tested through experimental observations (e.g. Plona, 1980). However, it is often reported that the Biot theory cannot adequately explain the large velocity dispersion and the strong attenuation in many rocks (Yang and Zhang, 2002). Furthermore, Biot theory does not take into account the effect of pore shape, which has significant influence on seismic wave propagation (e.g. Pham et al., 2002). Another attenuation mechanism due to fluid is the microscopic mechanism called the 'squirt-flow mechanism' (e.g. Dvorkin et al., 1995) which describes the effect on attenuation of pressure equilibration at the micro scale. Fluid flow from soft pores to stiff pores occurs in the pore pressure gradient due to a passing wave, which results in the dissipation of the passing wave. The mechanisms of fluid flow based on the Biot theory include viscous and inertial flows in the direction of wave propagation, while the mechanism of squirt flow includes viscous flow perpendicular to the direction of wave propagation (Figure 7). Our future studies should take such mechanisms into account to develop a more plausible mechanism for attenuation in ice-brine coexisting systems.

Attenuation of ultrasonic waves measured in our experiment is due not only to the intrinsic attenuation of the ice-brine coexisting system, but also to wave scattering. Scattering attenuation is caused by elastic wave scattering from velocity and density heterogeneities. The level of scattering attenuation is related to the scale of the heterogeneity of acoustic impedance between ice and unfrozen brine. If the wavelength of the seismic wave is much longer than the scale length of heterogeneity in an ice-brine coexisting system, the system is considered to be a homogeneous material. The intrinsic component of attenuation is important in characterising the physical properties of subsurface formations, but distinguishing between intrinsic attenuation and scattering attenuation is typically difficult. Hackert and Parra (2003) characterised the microstructure from X-ray computerised-tomography scans of carbonate cores, and then used 3D finite-difference modelling to determine the frequency-dependent scattering attenuation of P-wave in these cores at ultrasonic frequencies. They concluded that the predicted scattering attenuation is quite high. For further investigation of the scattering attenuation in an ice-brine coexisting system, it may be helpful to estimate pore morphology by non-destructive methods such as a magnetic resonance imaging (MRI) technique.

Carcione et al. (2007) used Biot's poroelastic model (Biot, 1956) to describe the propagation of ultrasonic waves through partially frozen orange juice, which is a solid-liquid coexistence system. They predicted the degree of freezing of orange juice by using the wave velocity and attenuation factor. Their theoretical results were compared with the experimental results obtained by Lee et al. (2004) who characterised the ultrasonic wave properties of orange juice, specifically velocity and attenuation coefficient, as the temperature was reduced from 20°C to −50°C. The waveform analyses by Lee et al. (2004) demonstrate that the ultrasonic attenuation coefficient in an ice-liquid coexisting system reaches its peak at the onset of freezing (−20°C), at which the formation of ice crystals begins and accelerates with a reduction in temperature, resulting in a mixture of ice and unfrozen water. Furthermore, the attenuation coefficient would decrease abruptly at temperatures below −20°C because of the decrease in unfrozen water and the growth of ice crystals. However, the P-wave velocity in the juice decreased slightly till −10°C in a liquid state. However, below −10°C the velocity first rose abruptly as ice crystals formed. Then, as the temperature continued to decrease, the P-wave velocity increased more gradually with further decreasing temperature. These results are similar to those reported in Matsushima et al. (2008). Finally, Carcione et al. (2007) concluded that the model shows a good agreement with the experimental data on wave velocities, and a qualitative agreement with the experimental attenuation values. In this case, the seismic scattering effect can be neglected because the scale length of heterogeneity in an ice-liquid coexisting system may be much smaller than the wavelength. Lee et al. (2002) obtained MR images of partially frozen orange juice with a pixel resolution of 0.7 mm × 0.7 mm. According to those MR images, the degree of heterogeneity of a solid-liquid coexistence system seems not to be large. In addition, one should also note that the dominant frequency (5 MHz) used in the experiments conducted by Lee et al. (2004) is nearly 10 times higher than that used in Matsushima et al. (2008).

In order to understand the seismic attenuation mechanisms and quantify MHs, a three-phase model is needed. Leclaire et al. (1994) expanded Biot's model to analyse wave propagation in frozen porous media such as frozen soil and permafrost. In their model, ice particles and liquid water coexist, and elastic waves propagate through a three-phase mixture of a solid grain matrix, liquid water, and a solid ice matrix (Figure 8). In Figure 8, they assume that the solid substrate and ice were not in direct contact; that is, a film of unfrozen water existed around the ice isolating it from sediments, so that friction did not occur between the

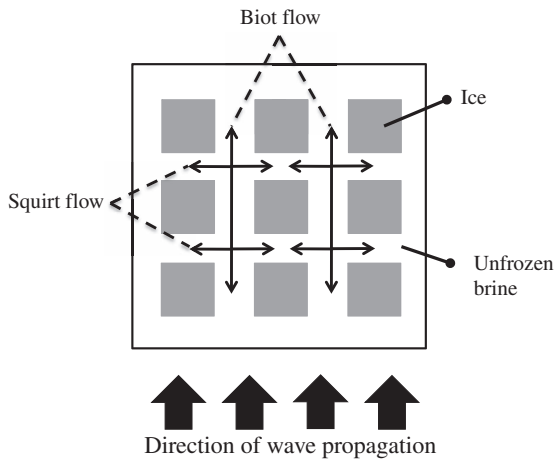

Fig. 7. Schematic illustration of the Biot and squirt flow mechanisms in the idealised ice-brine coexisting system. The motion of fluid is parallel to the direction of a planar P-wave propagation in the Biot mechanism while the motion of fluid is perpendicular the direction of a planar P-wave propagation in the squirt mechanism.

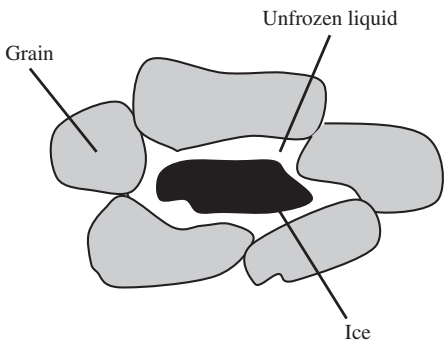

Fig. 8. Ice formation in frozen porous media. A layer of unfrozen water exists around the solid particles isolating them from ice.

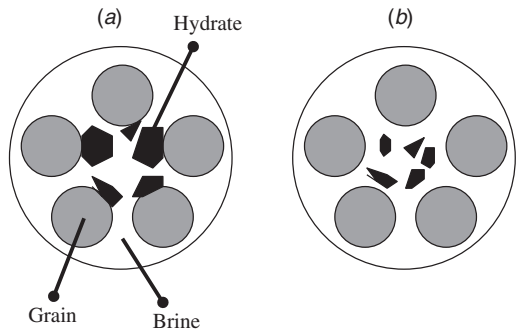

Fig. 9. Variations of micro-scale MH distribution in pore spaces: (*a*) contacting model, and (*b*) suspending model.

sediments and ice. Tada and Kimura (1999) conducted laboratory measurements with a glass-beads-packed medium. They compared observed compressional and shear wave velocities with theoretical velocities derived from the three-phase porous model proposed by Tada (1999) and found moderate correlation between them. Their physical model is similar to that of Leclaire et al. (1994), that is, there is no friction between sediments and ice. There are many variations of micro-scale MH distribution in pore spaces. If the hydrate forms at grain contacts (Figure 9*a*), it may act as a component of the load-bearing sediment framework and stiffen the sediment framework (e.g. Helgerud et al., 1999). In this case, both compressional and shear wave velocities will increase dramatically, even if MH occupies only a small percentage of the pore space. If the hydrate were suspended in pore spaces with no grain contact (Figure 9*b*), the hydrate content would mainly affect the elastic moduli and bulk density of the pore fluid, having little effect on the strength of the sediment framework. In this case, the compressional wave velocity will increase only slightly, while the shear wave velocity will also increase only slightly. Guerin and Goldberg (2005) added physical interactions between the solid and fluid phases to Leclaire's model (1994), such as cementation by elastic shear coupling and squirt flow squeezed laterally by a passing wave. Our future studies should take such a three-phase system into account to develop a more plausible mechanism for attenuation in hydrate-bearing sediments.

Conclusions

In terms of a plausible mechanism for intrinsic attenuation in ice-brine coexisting systems, we used the poroelastic model based on Biot theory to describe the propagation of ultrasonic waves through partially frozen media. In order to reduce the uncertainty of unknown physical parameters such as porosity and viscosity, possible physical parameters of partially frozen brines were used to calculate theoretical velocity and attenuation. Although the poroelastic model does not completely explain the measured attenuation results from an experimental study, the model partly explains the attenuation mechanism in an ice-brine coexisting system. It is often indicated that the Biot theory cannot adequately explain the strong attenuation. Our future studies should take other mechanisms such as squirt-flow mechanism and scattering effect into account to develop a more plausible mechanism for attenuation in ice-brine coexisting systems.

Acknowledgments

This study was supported by a Grant-in-Aid for Scientific Research from the Ministry of Education, Culture, Sports, Science and Technology of Japan (Grant No. 18686073) and also supported by JOGMEC (Japan Oil, Gas and Metals National Corporation) under the joint research program between JOGMEC and The University of Tokyo. The authors also thank two anonymous reviewers for their constructive comments, which largely improved the quality of our manuscript.

References

Berryman, J. G., 1980, Confirmation of Biot's Theory: *Applied Physics Letters*, **37**, 382–384. doi:10.1063/1.91951

Biot, M. A., 1956, Theory of propagation of elastic waves in a fluid saturated porous solid, I. Low-Frequency Range and II. High-Frequency range: *The Journal of the Acoustical Society of America*, **28**, 168–191. doi:10.1121/1.1908239

Burridge, R., and Keller, J. B., 1981, Poroelasticity equations derived from microstructure: *The Journal of the Acoustical Society of America*, **70**, 1140–1146. doi:10.1121/1.386945

Callaghan, P. T., Dykstra, R., Eccles, C. D., Haskell, T. G., and Seymour, J. D., 1999, A nuclear magnetic resonance study of Antarctic sea ice brine diffusivity: *Cold Regions Science and Technology*, **29**, 153–171. doi:10.1016/S0165-232X(99)00024-5

Carcione, J. M., and Seriani, G., 2001, Wave simulation in frozen porous media: *Journal of Computational Physics*, **170**, 676–695. doi:10.1006/jcph.2001.6756

Carcione, J. M., Santos, J. E., Ravazzoli, C. L., and Helle, H. B., 2003, Wave simulation in partially frozen porous media with fractal freezing conditions: *Journal of Applied Physics*, **94**, 7839–7847. doi:10.1063/1.1606861

Carcione, J. M., Campanella, O. H., and Santos, J. E., 2007, A poroelastic model for wave propagation in partially frozen orange juice: *Journal of Food Engineering*, **80**, 11–17. doi:10.1016/j.jfoodeng.2006.04.044

Carman, P. C., 1937, Fluid flow through a granular bed: *Transactions of the Institution of Chemical Engineers*, **15**, 150–166.

Carr, H. Y., and Purcell, E. M., 1954, Effects of diffusion on free precession in nuclear magnetic resonance experiments: *Physical Review*, **94**, 630–638. doi:10.1103/PhysRev.94.630

De Gennes, P. G., 1976, On a relation between percolation theory and the elasticity of gels: *Journal de Physique Lettres*, **37**, 1–2. doi:10.1051/jphyslet:019760037010100

Deptuck, D., Harrison, J. P., and Zawadzki, P., 1985, Measurement of elasticity and conductivity of a three-dimensional percolation system: *Physical Review Letters*, **54**, 913–916. doi:10.1103/PhysRevLett.54.913

Dvorkin, J., Mavko, G., and Nur, A., 1995, Squirt flow in fully saturated rocks: *Geophysics*, **60**, 97–107. doi:10.1190/1.1443767

Ecker, C., Dvorkin, J., and Nur, M. A., 2000, Estimating the amount of gas hydrate and free gas from marine seismic data: *Geophysics*, **65**, 565–573. doi:10.1190/1.1444752

Gao, L., Poirier, J., and Aki, K., 1993, Attenuation due to partial melting: an experimental study on a model system, using the lab coda method: *Journal of Geophysical Research*, **98**, 1853–1860. doi:10.1029/92JB02296

Gassmann, F., 1951, Über der Elastizität poröser Medien: *Vieteljahrsschrift der Naturforschenden. Gesellschaft in Zurich*, **96**, 1–23.

Guerin, G., and Goldberg, D., 2002, Sonic waveform attenuation in gas hydrate-bearing sediments from the Mallik 2L–38 research well, Mackenzie Delta, Canada: *Journal of Geophysical Research*, **107**, 2088. doi:10.1029/2001JB000556

Guerin, G., and Goldberg, D., 2005, Modeling of acoustic wave dissipation in gas hydrate - bearing sediments: *Geochemistry Geophysics Geosystems*, **6**, Q07010. doi:10.1029/2005GC000918

Hackert, C. L., and Parra, J. O., 2003, Estimating scattering attenuation from vugs or karsts: *Geophysics*, **68**, 1182–1188. doi:10.1190/1.1598111

Helgerud, M., Dvorkin, J., Nur, A., Sakai, A., and Collett, T., 1999, Elastic-wave velocity in marine sediments with gas hydrates: effective medium modelling: *Geophysical Research Letters*, **26**, 2021–2024. doi:10.1029/1999GL900421

Johnson, D. L., Koplik, J., and Dashen, R., 1987, Theory of dynamic permeability and tortuosity in fluid-saturated porous media: *Journal of Fluid Mechanics*, **176**, 379–402. doi:10.1017/S0022112087000727

Johnston, D. H., Toksöz, M. N., and Timur, A., 1979, Attenuation of seismic waves in dry and saturated rocks: II. Mechanisms: *Geophysics*, **44**, 691–711. doi:10.1190/1.1440970

Korenaga, J., Holbrook, W. S., Singh, S. C., and Minshull, T. A., 1997, Natural gas hydrates on the Southeast U.S. margin: Constraints from full-waveform and travel time inversion of wide-angle seismic data: *Journal of Geophysical Research*, **102**, 15345–15365. doi:10.1029/97JB00725

Kozeny, J., 1927, Über kapillare Leitung des Wassers im Boden – Aufstieg, Versickerung und Anwendung auf die Bewässerung, Sitzungsberichte der Akademie der Wissenschaften Wien: *Mathematisch Naturwissenschaftliche Abteilung*, **136**, 271–306.

Klimentos, T., and McCann, C., 1990, Relationships between compressional wave attenuation, porosity, clay content, and permeability of sandstone: *Geophysics*, **55**, 998–1014. doi:10.1190/1.1442928

Leclaire, P., Cohen-Tenoudji, F., and Aguirre-Puente, J., 1994, Extension of Biot's theory of wave propagation to frozen porous media: *The Journal of the Acoustical Society of America*, **96**, 3753–3768. doi:10.1121/1.411336

Lee, M. W., 2006, Is amplitude loss of sonic waveforms due to intrinsic attenuation or source coupling to the medium? *Scientific Investigations Report 2006–5120*, 13 pp., U.S. Geological Survey, Reston, Virginia.

Lee, S., Cornillon, P., and Kim, Y., 2002, Spatial investigation of the nonfrozen water distribution in frozen foods using NMR SPRITE: *Journal of Food Science*, **67**, 2251–2255. doi:10.1111/j.1365-2621.2002.tb09536.x

Lee, S., Pyrak-Nolte, L. J., Cornillon, P., and Campanella, O., 2004, Characterization of frozen orange juice by ultrasound and wavelet analysis: *Journal of the Science of Food and Agriculture*, **84**, 405–410. doi:10.1002/jsfa.1558

Matsushima, J., 2005,, Attenuation measurements from sonic waveform logs in methane hydrate-bearing sediments at the Nankai Trough exploratory well off Tokai, central Japan: *Geophysical Research Letters*, **32**, L03306. (Correction): *Geophysical Research Letters*, **33**, L02305. doi:10.1029/2005GL024466

Matsushima, J., 2006, Seismic wave attenuation in methane hydrate-bearing sediments: Vertical seismic profiling data from the Nankai Trough exploratory well, offshore Tokai, central Japan: *Journal of Geophysical Research*, **111**, B10101. doi:10.1029/2005JB004031

Matsushima, J., Suzuki, M., Kato, Y., Nibe, T., and Rokugawa, S., 2008, Laboratory experiments on compressional ultrasonic wave attenuation in partially frozen brines: *Geophysics*, **73**, N9–N18.

Meiboom, S., and Gill, D., 1958, Modified spin-echo method for measuring nuclear relaxation times: *The Review of Scientific Instruments*, **29**, 688–691. doi:10.1063/1.1716296

Pham, N. H., Carcione, J. M., Helle, H. B., and Ursin, B., 2002, Wave velocities and attenuation of shaley sandstones as a function of pore pressure and partial saturation: *Geophysical Prospecting*, **50**, 615–627. doi:10.1046/j.1365-2478.2002.00343.x

Plona, T. J., 1980, Observation of a second bulk compressional wave in a porous medium at ultrasonic frequencies: *Applied Physics Letters*, **36**, 259–261. doi:10.1063/1.91445

Prasad, M., and Dvorkin, J., 2004, Velocity and attenuation of compressional waves in brines: *74th Annual International Meeting, SEG, Expanded Abstracts*, **23**, 1666–1669.

Pratt, R., Bauer, K., and Weber, M., 2003, Crosshole waveform tomography velocity and attenuation images of arctic gas hydrates: *73rd SEG Annual Meeting, Extended Abstracts*, **22**, 2255–2258.

Priest, J. A., Best, A. I., and Clayton, C. R. I., 2006, Attenuation of seismic waves in methane gas hydrate-bearing sand: *Geophysical Journal International*, **164**, 149–159. doi:10.1111/j.1365-246X.2005.02831.x

Sams, M., and Goldberg, D., 1990, The validity of Q estimates from borehole data using spectral ratios: *Geophysics*, **55**, 97–101. doi:10.1190/1.1442776

Spetzler, H., and Anderson, D. L., 1968, The effect of temperature and partial melting on velocity and attenuation in a simple binary system: *Journal of Geophysical Research*, **73**, 6051–6060. doi:10.1029/JB073i018p06051

Sloan, E. D., 1990, Clathrate Hydrates of Natural Gases: Marcel Dekker.

Stoll, R. D., 1977, Acoustic waves in ocean sediments: *Geophysics*, **42**, 715–725. doi:10.1190/1.1440741

Suzuki, M., Matsushima, J., Kato, Y., Nibe, T., and Rokugawa, S., 2010, Ultrasonic wave-transmission measurement system on an ice-brine coexisting system: *Butsuri Tansa*, **63**, 239–249. [in Japanese with English abstract]

Tada, R., 1999, Experimental study of the elastic wave propagation in the granular composite material: *Butsuri Tansa*, **52**, 28–42. [in Japanese with English abstract]

Tada, R., and Kimura, M., 1999, Experimental study of the elastic wave propagation in composite porous media with glass beads and ice constituents – comparison with numerical study: *Butsuri Tansa*, **52**, 323–335. [in Japanese with English abstract]

Walsh, J. B., 1966, Seismic attenuation in rock due to friction: *Journal of Geophysical Research*, **71**, 2591–2599.

Walsh, J. B., 1969, New analysis of attenuation in partially melted rock: *Journal of Geophysical Research*, **74**, 4333–4337. doi:10.1029/JB074i017p04333

Winkler, K. W., and Nur, A., 1982, Seismic attenuation: Effects of pore fluids and frictional sliding: *Geophysics*, **47**, 1–15. doi:10.1190/1.1441276

Wood, W. T., Stoffa, P. L., and Shipley, T. H., 1994, Quantitative detection of methane hydrate through high-resolution seismic velocity analysis: *Journal of Geophysical Research*, **99**, 9681–9695. doi:10.1029/94JB00238

Yang, D., and Zhang, Z., 2002, Poroelastic wave equation including the Biot/squirt mechanism and the solid/fluid coupling anisotropy: *Wave Motion*, **35**, 223–245. doi:10.1016/S0165-2125(01)00106-8

Manuscript received 25 August 2010; accepted 30 November 2010.

部分凍結した塩水における超音波減衰の岩石物理学的研究

松島　潤[1]・新部貴夫[2]・鈴木　誠[1]・加藤俶史[1]・六川修一[3]

1 東京大学大学院工学系研究科　エネルギー・資源フロンティアセンター
2 東京大学大学院工学系研究科（現・(株)地球科学総合研究所）
3 東京大学大学院工学系研究科　技術経営戦略学専攻

要　旨：　流体を含む混成物における地震波内部減衰に対しては多くの減衰メカニズムが指摘されているが、固体と液体の相互作用が最も重要である。我々は過去の研究において、固液共存系における超音波伝播実験を実施し、微小空間に存在する不凍水が波動伝播に与える影響を調べた。様々な温度で測定された超音波減衰結果（周波数範囲：350−600 kHz）を説明するための物理的メカニズムを解明するために、Biot 理論に基づく多孔質弾性モデルを使用した。固相を氷、液相を不凍塩水と仮定することにより、核磁気共鳴技術で測定された液体特性を用いて孔隙率を計算した。周波数 500 kHz で計算された内部減衰値は、室内実験で測定された固液共存系の減衰値を説明するには十分ではないことがわかった。このことは、squirt 流れによる減衰メカニズムや散乱減衰などの他の減衰メカニズムを考慮する必要があることを示唆する。

キーワード：多孔質弾性，部分固結塩水，超音波減衰，Biot 理論，減衰メカニズム

부분 동결된 소금물에서의 초음파감쇠에 대한 다공성탄성 모델

Jun Matsushima[1], Takao Nibe[1,2], Makoto Suzuki[1], Yoshibumi Kato[1], Shuichi Rokugawa[3]

1 동경대학 대학원 공학계 연구과 에너지 자원 프론티어 센터
2 동경대학 대학원 공학계 연구과 (현 JGI Inc.)
3 동경대학 대학원 공학계 연구과 기술경영전략학 전공

요 약：　유체를 포함하는 혼합 매질에서의 탄성파 고유 감쇠에 대한 다양한 메커니즘 중, 탄성파 전파 시 고체와 유체 사이에서의 상대적 운동은 가장 중요한 감쇠 메커니즘 중의 하나이다. 선행 연구에서는 얼음의 미세 공극 안에 존재하는 소금물이 초음파의 전파에 미치는 영향을 분석하기 위하여 얼음과 소금물이 공존하는 매질에서 초음파 전파 실험하였다. 부분적으로 동결된 소금물에서 각기 다른 온도에서의 초음파 감쇠의 물리적인 메커니즘을 350 ~ 600 kHz의 주파수 대역에서 규명하기 위하여, Biot 이론에 입각한 다공성의 탄성 모델을 도입하여 초음파의 전파를 측정하였다. 고체상은 얼음으로, 액체상은 소금물로 가정한 뒤 펄스 핵자기공명기술로 측정한 유체의 성질을 이용하여 각각의 온도에서의 공극률을 계산한 결과, 실험으로 측정한 감쇠값은 500 kHz에서 계산된 고유 감쇠값과 다르게 나타났으며 이는 squirt-flow 메커니즘과 파의 산란 효과와 같은 다른 감쇠 메커니즘도 고려해야 한다는 것을 의미한다.

주요어： 탄성다공, 부분 동결된 소금물, 초음파 감쇠, Biot 이론, 감쇠 메커니즘